THE JOURNAL OF BIOLOGICAL CHEMISTRY VOL. 282, NO. 18, pp. 13573–13584, May 4, 2007

Molecular Basis of Selectivity of Nucleoside Triphosphate Incorporation Opposite O^6-Benzylguanine by *Sulfolobus solfataricus* DNA Polymerase Dpo4

STEADY-STATE AND PRE-STEADY-STATE KINETICS AND X-RAY CRYSTALLOGRAPHY OF CORRECT AND INCORRECT PAIRING[*] [S]

Received for publication, January 23, 2007, and in revised form, March 2, 2007 Published, JBC Papers in Press, March 3, 2007, DOI 10.1074/jbc.M700656200

Robert L. Eoff[‡§], **Karen C. Angel**[‡§], **Martin Egli**[‡§], **and F. Peter Guengerich**[‡§1]

From the Departments of [‡]*Biochemistry and* [§]*Center in Molecular Toxicology, Vanderbilt University School of Medicine, Nashville, Tennessee 37232-0146*

Previous work has shown that *Sulfolobus solfataricus* DNA polymerase Dpo4-catalyzed bypass of O^6-methylguanine (O^6-MeG) proceeds largely in an accurate but inefficient manner with a "wobble" base pairing between C and O^6-MeG (Eoff, R. L., Irimia, A., Egli, M., and Guengerich, F. P. (2007) *J. Biol. Chem.* 282, 1456–1467). We considered here the bulky lesion O^6-benzylguanine (O^6-BzG) in DNA and catalysis by Dpo4. Mass spectrometry analysis of polymerization products revealed that the enzyme bypasses and extends across from O^6-BzG, with C the major product (~70%) and some T and A (~15% each) incorporated opposite the lesion. Steady-state kinetic parameters indicated that Dpo4 was 7-, 5-, and 27-fold more efficient at C incorporation opposite O^6-BzG than T, A, or G, respectively. In transient state kinetic analysis, the catalytic efficiency was decreased 62-fold for C incorporation opposite O^6-BzG relative to unmodified DNA. Crystal structures reveal wobble pairing between C and O^6-BzG. Pseudo-"Watson-Crick" pairing was observed between T and O^6-BzG. Two other structures illustrate a possible mechanism for the accommodation of a +1 frameshift in the Dpo4 active site. The overall effect of O^6-BzG is to decrease the efficiency of bypass by roughly an order of magnitude in every case except correct bypass, where the effect is not as pronounced. By comparison, Dpo4 is more accurate but no more efficient than model replicative polymerases, such as bacteriophage T7$^-$ DNA polymerase and human immunodeficiency virus-1 reverse transcriptase in the polymerization past O^6-MeG and O^6-BzG.

Alkyl and aryl modifications are some of the most extensively studied forms of DNA damage (1), with O^6-alkylation providing one of the more mutagenic examples of this type of lesion (2, 3). Alkylating agents have been used in warfare (*i.e.* mustard gas), and they also continue to be used in chemotherapeutic regimes (4–6). Endogenous sources of DNA alkylation can arise through nonenzymatic methylation by *S*-adenosylmethionine, although O^6-alkylation is presumed to occur to only trace extents (7). Cellular repair of O^6-alkylation can result from the activity of O^6-alkylG DNA-alkyltransferases as well as mismatch repair pathways (8–10). If O^6-alkylation (or almost any type of DNA damage for that matter) is encountered by the replisome, then replication can be impeded or stopped completely. The geometric constraints placed upon the active site of "high fidelity" polymerases often translate into an inability to effectively bypass certain types of DNA damage (11). The Y-family DNA polymerases, on the other hand, appear to be well adapted toward translesion synthesis across many types of modified DNA.

Many studies have focused on DNA polymerase bypass of O^6-alkylG[2] lesions, most concerning bypass of the mutagenic O^6-MeG lesion (12–17). A recent study from our own group showed that the human replicative pol δ bypass of O^6-alkylG (including MeG, BzG, and PobG) was inhibited in very much the same manner as several human Y-family polymerases (including pol η, ι, and κ) (18). In general, relatively little preference was observed in steady-state reactions for either C or T insertion opposite O^6-alkylG with any of the polymerases tested, consistent with what has been reported with other polymerases. One notable difference was observed between pol δ

* This work was supported by National Institutes of Health Grants R01 ES010375 (to F. P. G.), F32 CA119776 (to R. L. E.), P30 ES000267 (to F. P. G. and M. E.), and P01 ES05355 (to M. E.). The costs of publication of this article were defrayed in part by the payment of page charges. This article must therefore be hereby marked "*advertisement*" in accordance with 18 U.S.C. Section 1734 solely to indicate this fact.

The atomic coordinates and structure factors (code 2jef, 2jeg, 2jei, and 2jej) have been deposited in the Protein Data Bank, Research Collaboratory for Structural Bioinformatics, Rutgers University, New Brunswick, NJ (http://www.rcsb.org/).

[S] The on-line version of this article (available at http://www.jbc.org) contains supplemental Figs. S1–S8 and Tables S1–S6, which document the purity of the O^6-BzG oligonucleotides that were used in this study. The supplemental data also contain a significant portion of the LC-MS/MS results used to analyze full-length extension by Dpo4.

[1] To whom correspondence should be addressed: Dept. of Biochemistry and Center in Molecular Toxicology, Vanderbilt University School of Medicine, 638 Robinson Research Bldg., 23rd and Pierce Aves., Nashville, TN 37232-0146. Tel.: 615-322-2261; Fax: 615-322-3141; E-mail: f.guengerich@vanderbilt.edu.

[2] The abbreviations used are: alkylG, alkylguanine; MeG, methylguanine; BF, *B. stearothermophilus* DNA polymerase I, large fragment; BSA, bovine serum albumin; BzG, benzylguanine; CID, collision-induced dissociation; dCTPαS, 2′-deoxycytidine 5′-*O*-(1-thiotriphosphate); DTT, dithiothreitol; HIV-1, human immunodeficiency virus-1; LC, liquid chromatography; MS, mass spectrometry; MS/MS, tandem mass spectrometry; PobG, 4-oxo-4-(3-pyridyl)butylguanine; pol, (DNA) polymerase; pol T7$^-$, bacteriophage pol T7 exonuclease-deficient; RT, reverse transcriptase; UDG, uracil DNA glycosylase; r.m.s., root mean square. The generic term "alkyl" is used to include both alkyl and aralkyl (Bz) groups for convenience.

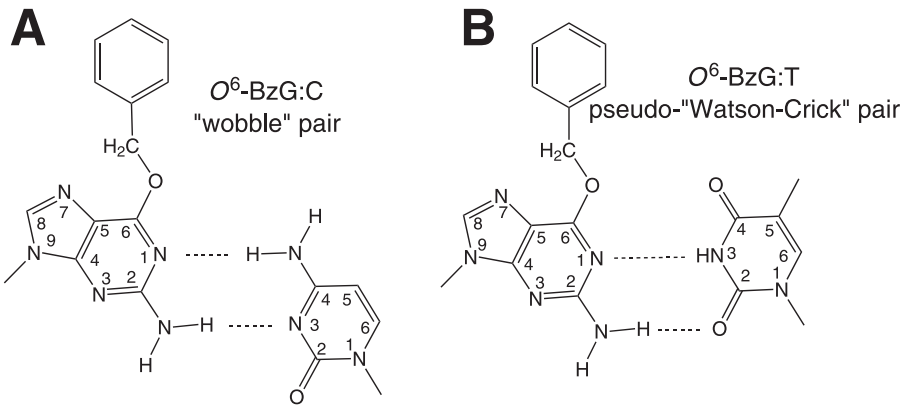

FIGURE 1. **Schematic representation of O^6-BzG modification and potential base pairing orientations.** *A*, O^6-BzG:C "wobble" base pair. *B*, O^6-BzG:T pseudo-Watson-Crick base pair.

and the Y-family polymerases. No primer extension was observed when pol δ encountered O^6-PobG, in contrast to pol η, which was able to extend beyond the bulkiest lesion tested in largely an accurate manner (~80% correct bypass), suggestive of more geometric tolerance in the active site of pol η (18).

Dpo4 (DNA polymerase IV) from *S. solfataricus* P2 has served as a readily accessible source of mechanistic information and a useful model concerning how many different types of DNA damage may be handled by the Y-family polymerases (19–24). Recent work from our group has focused on *in vitro* Dpo4-catalyzed bypass of O^6-MeG modified DNA by combining transient-state kinetic and mass spectral analyses with x-ray crystallography (25). As in the case of yeast pol η (12), the major product for Dpo4 was correct incorporation of C opposite O^6-MeG, followed by unperturbed extension of the C:O^6-MeG pair. A crystal structure with Dpo4 revealed that a "wobble" base pair occurs between C and O^6-MeG in the polymerase active site (Fig. 1*A*). Dpo4-catalyzed incorporation of T and A opposite O^6-MeG constituted minor products observed in the mass spectral analysis (~20 and 10%, respectively). Steady-state kinetic parameters revealed that a much higher $K_{m,\mathrm{dTTP}}$ was the dominant factor affecting the ability of Dpo4 to insert a T opposite O^6-MeG. A crystal structure was solved for a complex representing next-base incorporation following insertion of T opposite O^6-MeG, but the primer T was found to be largely disordered and needed to be placed in three alternate conformations, including a pseudo-Watson-Crick pair (Fig. 1*B*), in order to account for the electron density observed in that region (25).

In an effort to better understand the features of greatest relevance to Y-family polymerase bypass of O^6-adducted guanine, we analyzed Dpo4-catalyzed bypass of O^6-BzG by combining transient-state kinetics and mass spectrometry with x-ray crystallographic studies. Benzylation of DNA is known to occur upon exposure to certain reactive chemicals, such as the esophageal carcinogen *N*-nitrosobenzylmethylamine (26, 27). Comparing the effect of O^6-BzG upon Dpo4 catalysis with that of other O^6-alkylG modifications can serve as an instructive probe for polymerase bypass mechanism(s) (28), but to date there is no structural information relating the O^6-BzG or other bulky O^6-alkylG lesions and polymerase catalysis. The results provided herein help to illustrate the differences between how replicative and bypass polymerases perform translesion synthesis opposite O^6-alkylG lesions, allowing mechanistic comparisons to be made between Dpo4 and results obtained with model replicative polymerases, such as pol T7$^-$ and HIV-1 RT (16, 17). Such comparisons can also provide a useful compass when considering the differences observed between human pol δ and pol η during bypass of bulky O^6-alkylG lesions (18).

EXPERIMENTAL PROCEDURES

Materials—Dpo4 was expressed in *Escherichia coli* and purified to electrophoretic homogeneity as described previously (29). All unlabeled dNTPs were obtained from Amersham Biosciences, S_p-dCTPαS was purchased from Biolog Life Science Institute (Bremen, Germany), and [γ-^{32}P]ATP was purchased from PerkinElmer Life Sciences. All unmodified oligonucleotides used in this work were synthesized by Midland Certified Reagent Co. (Midland, TX) and purified using high performance liquid chromatography by the manufacturer, with analysis by matrix-assisted laser desorption time-of-flight MS. Two template DNA sequences were used: 5′-TCATXGAATCCTTCCCCC-3′ (template 1) and 5′-TCACXGAATCCTTCCCCC-3′ (template 2), where X represents O^6-BzG. The O^6-BzG-modified oligonucleotides were prepared using a modification of the procedure described elsewhere (16, 18) and purified by denaturing polyacrylamide gel electrophoresis. The identity of the O^6-BzG oligonucleotides was confirmed by matrix-assisted laser desorption time-of-flight MS, and the purity was determined by capillary gel electrophoresis (supplemental Figs. S1 and S2). The 13-base primer sequence used in the kinetic analyses and the O^6-BzG:dGTP structure was 5′-GGGGGAAGGATTC-3′. The 13-base primer sequence used in the mass spectrometry analysis of full-length extension products was 5′-GGGGGAAGGAUTC-3′. The 14-base primer sequences used in the indicated kinetic assays and the crystal structures was 5′-GGGGGAAGGATTCC-3′ (note that for the O^6-BzG:ddC-1 and O^6-BzG:ddC-1 structures, the primer was dideoxy-terminated), and 5′-GGGGGAAGGATTCT-3′ was used for the O^6-BzG:T structure. All of the crystal structures used the template 2 sequence with cytosine located on the 5′-side of the O^6-BzG modification.

Full-length Extension Assay—A ^{32}P-labeled primer was annealed to either an unmodified or adducted template oligonucleotide by heating a 1:1 solution of oligonucleotide to 95 °C for 5 min and then slow cooling to room temperature. The primer was then incubated with Dpo4 and extended in the presence of the indicated dNTP(s). Each reaction was initiated by adding dNTP·Mg^{2+} (250 μM each dNTP and 5 mM $MgCl_2$) solution to a preincubated Dpo4·DNA complex (100 nM Dpo4 and 200 nM DNA). The reaction was carried out at 37 °C in 50 mM Tris-HCl (pH 7.4), 50 mM NaCl, 5 mM DTT, 100 μg μl^{-1} BSA, and 35% (v/v) glycerol. At the indicated time, 5-μl aliquots

were quenched with 50 μl of 500 mM EDTA (pH 9.0). The samples were then mixed with 100 μl of a 95% formamide, 20 mM EDTA solution and were separated on a 20% polyacrylamide (w/v)/7 M urea gel. Products were visualized and quantified using a phosphor imager screen and Quantity One™ software, respectively (Bio-Rad). Formation of an 18-base extension product from a 13-base primer was quantified by fitting the data to Equation 1,

$$f_{18\text{-mer}}(t) = A\left(1 - \sum_{r=1}^{n} \frac{((k_{obs})t)^{r-1}}{(r-1)!} e^{-(k_{obs})t}\right) + k_2 t \quad \text{(Eq. 1)}$$

where A represents the amount of product formed during the first binding event between Dpo4 and DNA, k_{obs} is an observed rate constant defining nucleotide incorporation, n is the number of incorporation events required to observe product formation, k_2 is the steady-state rate of nucleotide incorporation, and t is time. For all kinetic assays, the experiments were performed once, and all statistical values given indicate S.E. from the fit of the data.

Steady-state Kinetics—Dpo4 catalyzed single nucleotide incorporation was measured over a range of dNTP concentrations. All reactions were carried out at 37 °C in 50 mM Tris-HCl (pH 7.4) buffer containing 50 mM NaCl, 1.0 mM DTT, 50 μg μl^{-1} BSA, and 5% glycerol (v/v). Dpo4 (10 nM) was preincubated with DNA (100 nM), and the reaction was initiated by adding dNTP·Mg^{2+}. Aliquots were quenched with 500 mM EDTA (pH 9.0) after varying incubation times. Substrate and product DNA were separated by electrophoresis on a 20% polyacrylamide (w/v), 7 M urea gel. The products were then visualized using a phosphor imager and quantitated using Quantity One™ software (Bio-Rad). The initial portion of the velocity curve was fit to a linear equation in the program GraphPad Prism (GraphPad, San Diego, CA). The resulting velocity was plotted as a function of dNTP concentration and then fit to a hyperbola, correcting for enzyme concentration, to obtain estimates of k_{cat} and $K_{m,dNTP}$.

Transient-state Kinetics—All pre-steady-state experiments were performed using a KinTek RQF-3 model chemical quench-flow apparatus (KinTek Corp., Austin, TX) with 50 mM Tris-HCl (pH 7.4) buffer in the drive syringes. All quench flow experiments were carried out at 37 °C in a buffer containing 50 mM Tris-HCl (pH 7.4), 50 mM NaCl, 5 mM DTT, 100 μg μl^{-1} BSA, and 35% (v/v) glycerol. Polymerase catalysis was stopped via the addition of 500 mM EDTA (pH 9.0). Where indicated, competitor primer-template DNA (1 μM 13/18-mer) was included in the right syringe as a trap for protein, thereby creating single-turnover conditions even under enzyme limiting conditions. Substrate and product DNA were separated by electrophoresis on a 20% polyacrylamide (w/v), 7 M urea gel. The products were then visualized using a phosphor imager and quantitated using Quantity One™ software. Results obtained under single-turnover conditions were fit to Equation 2,

$$y = A(1 - e^{-k_{obs}t}) \quad \text{(Eq. 2)}$$

where A represents the product formed in the first binding event, k_{obs} is a rate constant defining polymerization under the conditions used for the experiment being analyzed, and t is time. Results obtained under conditions that allowed a second round of Dpo4·DNA binding and polymerase action were fit to Equation 3,

$$y = A(1 - e^{-k_{obs}t}) + k_{ss}t \quad \text{(Eq. 3)}$$

where k_{ss} represents a steady-state velocity of nucleotide incorporation.

LC-MS/MS Analysis of Oligonucleotide Products from Dpo4 Reactions—Dpo4 (5 μM) was preincubated with primer-template DNA (10 μM), and the reaction was initiated by the addition of dNTP (1 mM each) and $MgCl_2$ (5 mM) for a final volume of 100 μl. Dpo4 catalysis was allowed to proceed at 37 °C for 4 h in 50 mM Tris-HCl (pH 7.8, at 25 °C) buffer containing 50 mM NaCl, 1 mM DTT, 50 μg μl^{-1} BSA, and 5% glycerol (v/v). The reaction was terminated by extraction of the remaining dNTPs by using a size exclusion chromatography column (Bio-Spin 6 chromatography column) (Bio-Rad). Concentrated stocks of Tris-HCl, DTT, and EDTA were added to restore the concentrations to 50, 5, and 1 mM, respectively. Next, *E. coli* uracil DNA glycosylase (20 units; Sigma) was added, and the solution was incubated at 37 °C for 6 h to hydrolyze the uracil residue on the extended primer (29). The reaction mixture was then heated at 95 °C for 1 h in the presence of 0.25 M piperidine, followed by removal of the solvent by centrifugation under vacuum. The dried sample was resuspended in 100 μl of H_2O for MS analysis.

LC-MS/MS analysis was performed on a Waters Aquity ultraperformance liquid chromatography system (Waters, Milford, MA) connected to a Finnigan LTQ mass spectrometer (ThermoElectron Corp., San Jose, CA), operating in the electrospray ionization negative ion mode. An Aquity ultraperformance liquid chromatography BEH octadecylsilane (C_{18}) column (1.7 μm, 1.0 × 100 mm) was used with the following LC conditions. Buffer A contained 10 mM $NH_4CH_3CO_2$ plus 2% CH_3CN (v/v), and buffer B contained 10 mM $NH_4CH_3CO_2$ plus 95% CH_3CN (v/v). The following gradient program was used with a flow rate of 150 μl min^{-1}: 0–3 min, linear gradient from 100% A to 97% A, 3% B (v/v); 3–4.5 min, linear gradient to 80% A, 20% B (v/v); 4–5.5 min, linear gradient to 100% B; 5–5.5 min, hold at 100% B; 5.5–6.5 min, linear gradient to 100% A; 6.5–9.5 min, hold at 100% A. The temperature of the column was maintained at 50 °C. Samples were injected with an autosampler system. Electrospray ionization conditions were as follows: source voltage 4 kV, source current 100 μA, auxillary gas flow rate setting 20, sweep gas flow rate setting 5, sheath gas flow setting 34, capillary voltage −49 V, capillary temperature 350 °C, tube lens voltage −90 V. MS/MS conditions were as follows: normalized collision energy 35%, activation Q 0.250, activation time 30 ms. The doubly (negatively) charged species were generally used for CID analysis. The calculations of the CID fragmentations of oligonucleotide sequences were done using a program linked to the Mass Spectrometry Group of Medicinal Chemistry at the University of Utah (available on the World Wide Web at www.medlib.med.utah.edu/massspec). The nomenclature used in supplemental Tables S1–S6 has been described previously (30).

Crystallization of Dpo4·DNA Complexes—Dpo4 was concentrated to ~300–550 μM (~12–22 mg ml^{-1}) using a spin concentrator with a 10^4 M_r cut-off filter (Amicon) in 50 mM Tris-HCl (pH 7.4 at 25 °C) buffer containing 200 mM NaCl, 5 mM β-mercaptoethanol, and 10% glycerol (v/v). Dpo4 was then mixed with DNA (1:1.2 molar ratio), incubated at 37 °C for 10 min, centrifuged at 10^4 rpm for 5 min (Centrifuge 5415 C; Eppendorf) to remove insoluble material, and then placed on ice for 1 h prior to incubation with 1 mM d(N)TP and 5 mM $CaCl_2$. Calcium was used as a cofactor during crystallization, because magnesium (which facilitates polymerization during crystallization) failed to provide diffraction quality crystals under the conditions used here. Crystals were grown using the sitting drop vapor diffusion method by mixing 1 μl of complex with 1 μl of solution containing 5–10% polyethylene glycol 3350 (w/v) and 100 mM $Ca(OAc)_2$ and equilibrated against a well solution containing 25 mM Tris-HCl (pH 7.4 at 25 °C) buffer, 5–10% polyethylene glycol 3350 (w/v), 100 mM $Ca(OAc)_2$, and 2.5% glycerol (v/v). Crystals were soaked in mother liquor containing an additional 25% polyethylene glycol 3350 (w/v) and 15% ethylene glycol (v/v) and then swiped through paratone-N (Hampton Research, Aliso Viejo, CA) and flash frozen in a stream of liquid nitrogen.

X-ray Diffraction, Data Collection, and Structure Refinement—Diffraction data sets for Dpo4 ternary O^6-BzG:ddC-1, O^6-BzG:ddC-2, and O^6-BzG:G complexes were collected at 110 K using a synchrotron radiation wavelength of 1.0 Å on the ID-22 beamline at the Advanced Photon Source (Argonne, IL). Diffraction data for the Dpo4 ternary O^6-BzG:T complex was collected at 110 K using a synchrotron radiation wavelength of 0.98 Å on the X25 beamline at the National Synchrotron Light Source (Brookhaven, NY). Indexing and scaling were performed using XDS (31) or HKL2000 (32). All four structures indexed to the same space group and had very similar unit cell parameters.

Structure Determination and Refinement—The refined O^6-MeG:T model (25) was used as a starting model for the O^6-BzG structures removing the 14th base in the primer strand and replacing the O^6-MeG residue with G for the initial molecular replacement (substituting O^6-BzG in later rounds of refinement). In each instance, several rounds of rigid body refinement of the diffraction data, with gradually increasing resolution, optimized the initial positions of the models. The model was refined further using the CNS Solve package (version 1.1) (33), including simulated annealing, gradient minimization, individual occupancy, and refinement of individual isotropic temperature factors. Manual model building was performed using TURBO.[3]

RESULTS

Extension of Oligonucleotide Primers by Dpo4 in the Presence of All Four dNTPs—As a general measure of how Dpo4 catalysis is affected by O^6-BzG, a time course was performed under enzyme limiting conditions (Fig. 2). An observed rate constant defining five incorporation events can be measured by following the appearance of the fully extended 18-mer primer and fitting the data to Equation 1, where $n = 5$. The O^6-BzG modification decreased the amount of product formed in the first binding event (*i.e.* the "burst" amplitude) by ~40% relative to that observed previously with a DNA control (25), indicating that fewer Dpo4 molecules are able to fully extend the primer in the first attempt (Fig. 2). It is important to note that in the absence of any other evidence, the exact identity of the fully extended product is unknown.

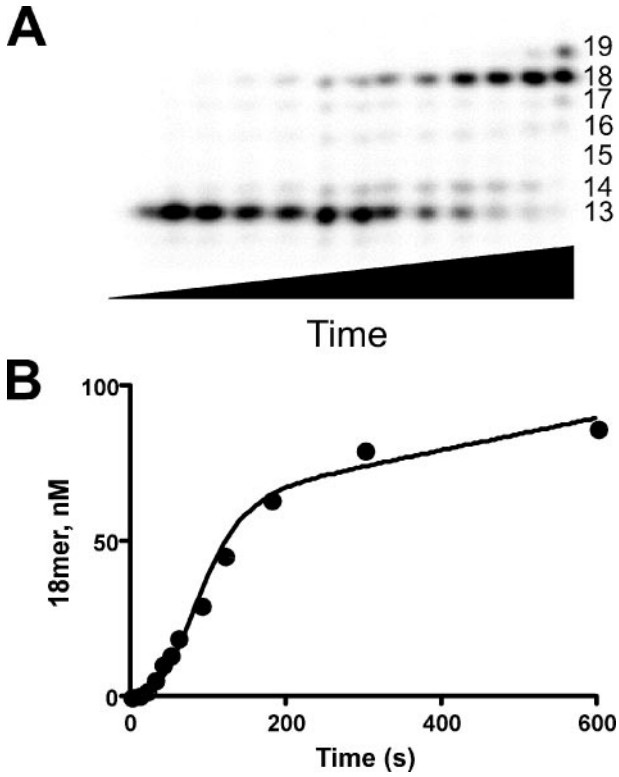

FIGURE 2. **Dpo4-catalyzed incorporation opposite and extension past O^6-MeG-adducted DNA.** *A*, Dpo4-catalyzed (100 nM) full-length extension of primer-template DNA (200 nM) containing O^6-BzG. The lengths of the oligonucleotide products are indicated on the *right*. *B*, plot of full-length product formation as a function of time with O^6-BzG (●). Results were fit to Equation 1 to yield the following kinetic parameters: $A = 58 \pm 6$ nM, $k_{obs} = 0.051 \pm 0.003$ s^{-1}, $k_2 = 0.052 \pm 0.013$ nM s^{-1} (k_2/[Dpo4] = 5.2×10^{-4} s^{-1}).

Dpo4 Catalysis in the Presence of a Single dNTP—Dpo4 catalysis was allowed to proceed in the presence of a single nucleotide. Dpo4 could incorporate all four dNTPs across from O^6-BzG adducts (supplemental Fig. S3). Steady-state kinetic assays were then employed as a first quantitative measure of the preferential mechanism for Dpo4 catalysis opposite O^6-BzG. The relative catalytic efficiency insertion opposite O^6-BzG by Dpo4 was then measured by varying the concentration of dNTP in the reaction solution (Table 1). The Dpo4 catalytic efficiency (k_{cat}/K_m) was strongly inhibited (~4900-fold) by the presence of O^6-BzG in the template DNA compared with ~950-fold reduction in Dpo4 catalysis opposite O^6-MeG (25). However, Dpo4 remains 5-, 7-, and 27-fold more efficient at correct incorporation of C opposite O^6-BzG compared with incorrect incorporation of T, A, or G opposite the lesion.

LC-MS/MS Analysis of Full-length Extension Products—Unambiguous identification of full-length extension products resulting from Dpo4 catalysis was carried out using an

[3] C. Cambillau and A. Roussel (1997) *Turbo Frodo*, Version OpenGL.1, Université Aix-Marseille II, Marseille, France.

TABLE 1
Steady-state kinetic parameters for 1-base incorporation by Dpo4

Oligomer pair	Template base	dNTP	k_{cat}	$K_{m,dNTP}$	ΔEfficiency relative to dCTP:G[a]
			s^{-1}	μM	
13-mer 18-mer-1	-G-	dCTP	0.58 ± 0.01[b]	3.0 ± 0.2[b]	
13-mer 18-mer-1	-O^6-BzG-	dCTP	0.055 ± 0.011	1400 ± 600	4,900-fold less
13-mer 18-mer-1	- O^6-BzG-	dTTP	0.0066 ± 0.0002	1200 ± 100	35,000-fold less
13-mer 18-mer-1	- O^6-BzG-	dATP	0.0025 ± 0.0003	300 ± 120	23,000-fold less
13-mer 18-mer-1	-O^6-BzG-	dGTP	0.00083 ± 0.00007	600 ± 160	138,000-fold less

[a] Change in efficiency describes the ratio of $(k_{cat}/K_{m,dNTP})_{dCTP:G}/(k_{cat}/K_{m,dNTP})_{dNTP:O^6\text{-}BzG}$.
[b] Data from Ref. 25.

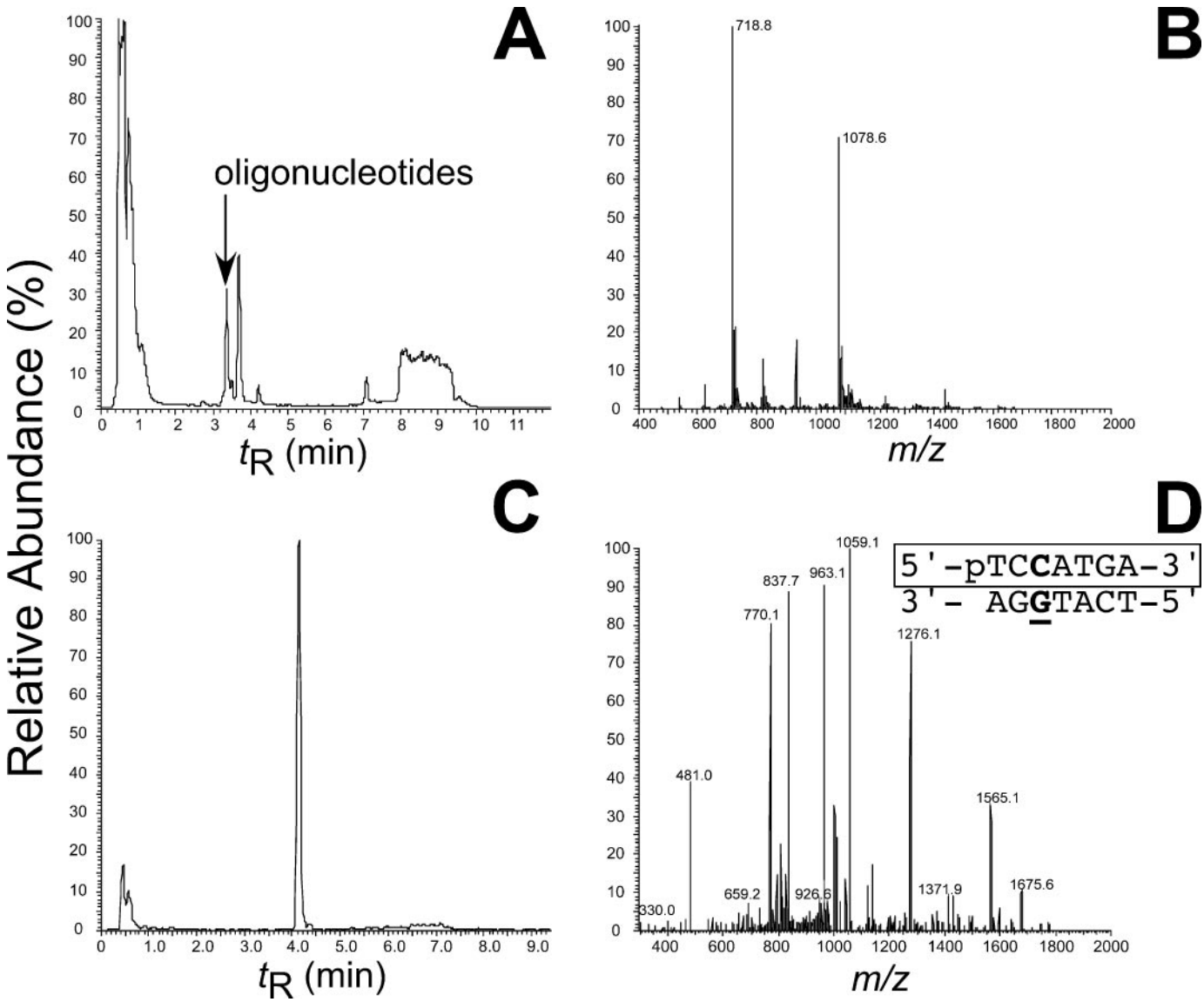

FIGURE 3. **Identification of Dpo4-catalyzed full-length extension products by LC-MS/MS.** *A*, total ion current trace of products derived from extension of 13/18-mer DNA containing O^6-BzG template 1. *B*, electrospray ionization mass spectrum of the oligonucleotide peaks that elute at 3.4 min. *C*, total ion current trace of ion *m/z* 1079. *D*, CID mass spectrum of ion *m/z* 1079. *G*, O^6-BzG. This product contained C inserted opposite O^6-BzG and extended in an error-free manner.

LC-MS/MS approach described previously (29). Two template sequences containing the modification were used in order to address potential sequence effects. Two major peaks were observed for template 1 and corresponded to ions at *m/z* 1079.0 and 718.8, which were −2 and −3 ions, respectively (Fig. 3*B*). Selected ion traces are shown in Fig. 3*C*, and CID analysis of the

m/z 1079 ion resulted in the fragmentation pattern shown in Fig. 3*D*. The major ions in the fragmentation pattern are consistent with the sequence 5′-pTCCATGA-3′, which corresponds to the insertion of C opposite O^6-BzG and accurate full-length extension of the primer (supplemental Table S1).

A second pair of ions was detected with template 1 at *m/z* 1086.2 and 723.8, both of which are consistent with the −2 and −3 charge states of a parent ion representing T insertion opposite template 1 O^6-BzG followed by accurate full-length extension. The third pair of ions detected at 1090.6 and 726.7 was consistent with the −2 and −3 charge states of a parent ion representing A insertion opposite template 1 O^6-BzG, followed by accurate full-length extension. CID provided a fragmentation pattern consistent with both minor product sequence assignments (supplemental Figs. S4 and S5 and Tables S2 and S3). Comparison of the selected ion counts for ions corresponding to all three products indicates that correct incorporation of C opposite O^6-BzG template 1 comprises roughly 70%, with T (~16%) and A (~14%) incorporation accounting for the remaining portion of products observed in the reaction mixture. This is consistent with what is observed in the steady-state parameters (Table 1). LC-MS/MS analysis of template 2 (differing only at the base 5′ to the O^6-BzG lesion) revealed a very similar product spectrum: ~70% C, ~14% T, and ~16% A incorporation (supplemental Figs. S6–S8 and Tables S4–S6).

Transient-state Kinetic Analysis for Dpo4 Bypass of O^6-BzG—Pre-steady-state experiments were performed under enzyme-limiting conditions (Dpo4/DNA = 1:2). The appearance of a rapid "burst" in product formation can provide a measure of the amount of active enzyme present in solution as well as an initial measure of the nucleotide incorporation rate opposite O^6-BzG by Dpo4. Based on previous work with unmodified DNA, essentially 100% of the Dpo4 is active under the experimental conditions used here. It should be noted that the same Dpo4 stock solution was used here as in the work with O^6-MeG) (25). The presence of O^6-BzG in the template strand resulted in a ~9% burst of product formation under the experimental conditions used here (Fig. 4*A*). The k_{obs} value is ~4-fold slower for incorporation opposite O^6-BzG compared with a previously determined value for undamaged DNA at the same concentration of dCTP (25).

Previously measured sulfur elemental ("thio") effects for unmodified G were ~1.9 (our group (25)) and ~1.4 from the Suo laboratory (19). For incorporation opposite O^6-BzG-modified DNA, substitution of dCTP with S_p-dCTPαS eliminated any observable burst in product formation (Fig. 4*A*), suggesting that phosphoryl transfer by Dpo4 is strongly inhibited in the presence of O^6-BzG-modified template DNA. Active site titration experiments were performed in order to assess the relative stability of Dpo4·O^6-BzG complexes when the enzyme is required to proceed through the phosphoryl transfer step (Fig. 4*B*). The apparent $K_{D,DNA}$ value for O^6-BzG is similar to both unmodified and O^6-MeG-modified DNA, indicating that O^6-BzG has no effect upon the intrinsic stability of the ternary complex (25).

To further assess the Dpo4 mechanism of O^6-BzG bypass, the concentration of dCTP in the reaction mixture was varied in order to measure the maximum forward rate constant

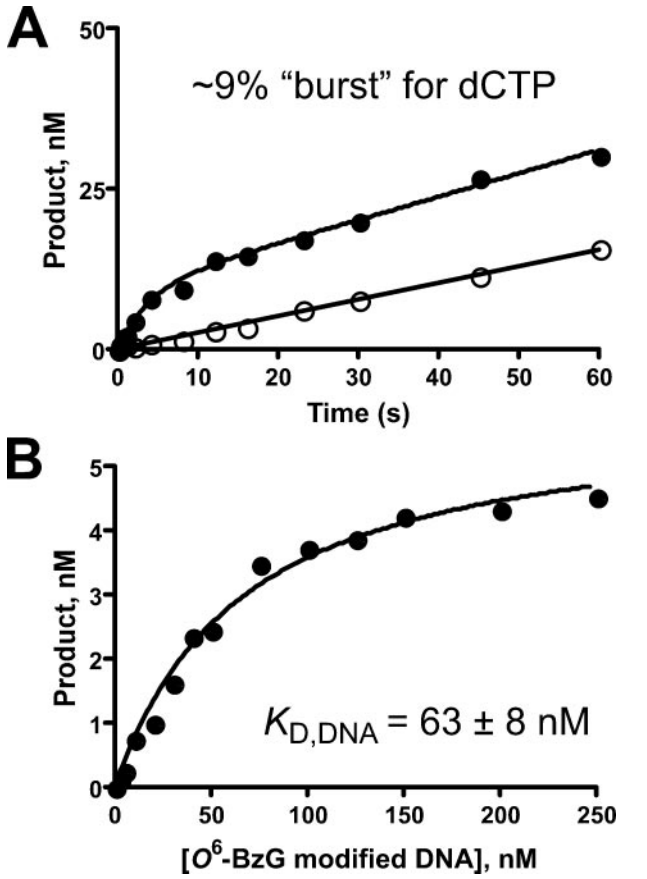

FIGURE 4. **Pre-steady-state analysis of Dpo4-catalyzed incorporation of dCTP.** *A*, Dpo4 (100 nM) was incubated with primer-template DNA (200 nM) containing O^6-BzG and 1 mM (●) dCTP or (○) S_p-dCTPαS. The results for (●) dCTP incorporation were then fit to Equation 2, and the following parameters were obtained. ●, dCTP, $A = 9 \pm 1$ nM, $k_{obs} = 0.28 \pm 0.06\ s^{-1}$, $k_{ss} = 0.36 \pm 0.02$ nM s^{-1}. The results for S_p-dCTPαS incorporation (○) were fit to a linear equation, which provides a steady-state rate of nucleotide incorporation, $k_{ss} = 0.25 \pm 0.01$ nM s^{-1}. *B*, single turnover product amplitude under enzyme-limiting conditions was plotted as a function of DNA concentration (2.5–250 nM). The results were then fit to a quadratic equation to obtain a measure of the apparent $K_{D,DNA}$. ●, O^6-BzG, $A = 5.9 \pm 0.3$ nM, $K_{D,DNA} = 63 \pm 8$ nM. The concentrations of Dpo4, dCTP, and unlabeled primer-template DNA trap were 25 nM, 1 mM, and 1 μM, respectively.

describing polymerization, k_{pol}, and the equilibrium dissociation constant, $K_{D,dCTP}$, which describes dCTP binding affinity of the Dpo4·DNA complex (Fig. 5*A*). Dpo4-catalyzed incorporation of dCTP opposite O^6-BzG-modified DNA proceeded at an ~6-fold slower rate relative to undamaged template, as evidenced by a decreased value of k_{pol} (Fig. 5*B* and Table 2). Strikingly, the apparent nucleotide binding affinity is ~11-fold less than that of unmodified G (*i.e.* $K_{D,dCTP}$ is roughly 11-fold higher for O^6-BzG). The overall catalytic efficiency (relative to dCTP insertion opposite G) was decreased 62-fold when Dpo4 inserts dCTP opposite O^6-BzG. Pre-steady-state kinetic analysis of dTTP misincorporation could not be determined due to an absence of any measurable amount of product formed in the first binding event under all conditions tested (Fig. 5*C*).

Perturbation of Incorporation Beyond an O^6-BzG:C Pair—In order to address the catalytic cycle that occurs immediately following incorporation opposite O^6-BzG, two synthetic 14-mer primers were used, one containing C paired opposite O^6-BzG and a second containing T paired opposite O^6-BzG.

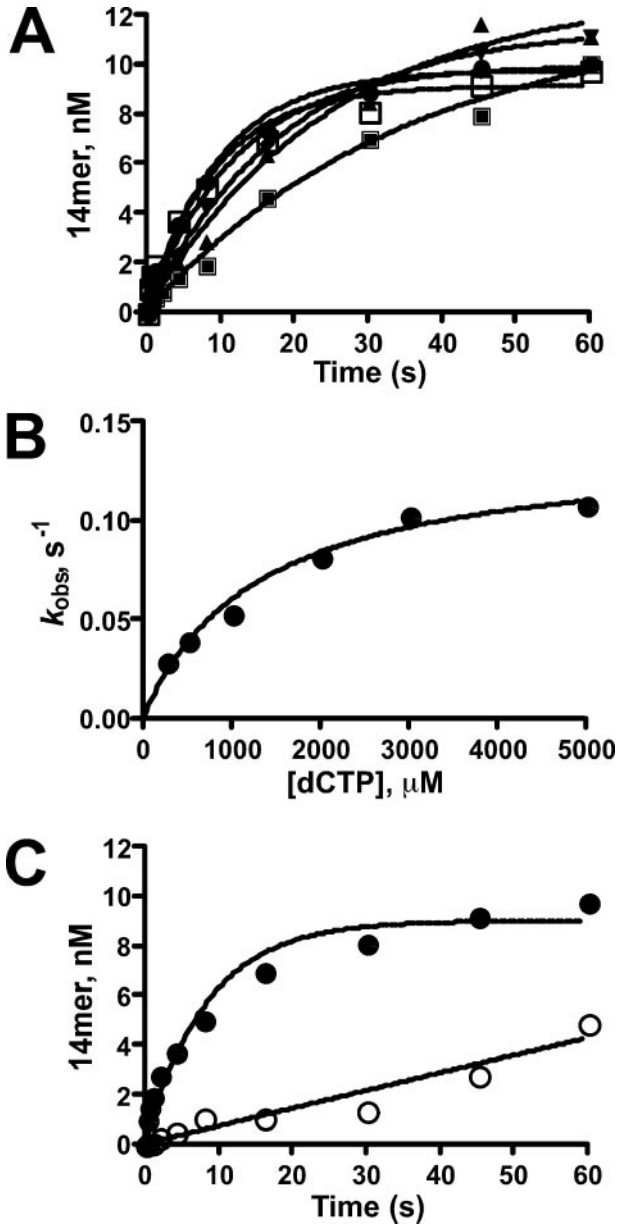

FIGURE 5. **Determination of k_{pol} and $K_{D,dCTP}$ for Dpo4-catalyzed incorporation of dCTP opposite O^6-BzG.** *A*, measurement of Dpo4-catalyzed incorporation opposite O^6-BzG at varying concentrations of dCTP (●). *B*, the observed rate of nucleotide incorporation was plotted as a function of dCTP concentration and fit to a quadratic equation to yield kinetic parameters (Table 2). *C*, comparison of Dpo4-catalyzed incorporation of 2.5 mM dCTP (●) and dTTP (○).

The maximum forward rate for correct incorporation of dATP was decreased ~1.5-fold relative to unmodified G and O^6-MeG when C was paired opposite O^6-BzG (Table 2). The next-base extension of the mispaired T:O^6-BzG proceeded at an ~2-fold slower forward rate than extension of the correct pairing of C opposite O^6-BzG (Table 2). The $K_{D,dCTP}$ was higher in both instances than observed for unmodified G. Comparison of the efficiency of next base extension revealed that extension of a correct C:O^6-BzG pairing was decreased 7-fold relative to unmodified G, whereas the efficiency for next base extension of a T:O^6-MeG mispair was decreased ~24-fold. The overall trend with O^6-BzG was similar to what was observed with O^6-MeG, but the level of inhibition at each step is greater for O^6-BzG.

Dpo4-catalyzed incorporation opposite the O^6-BzG lesion was impeded regardless of the nucleotide being inserted, but misincorporation events were clearly inhibited to a greater degree (Table 1). Similar to results with O^6-MeG, the rate of phosphoryl transfer appeared to be inhibited by O^6-BzG.

Postinsertion Ternary Complex for "Correct" Bypass of O^6-BzG—Crystallization experiments were performed for all potential pairings opposite O^6-BzG. Crystal growth was improved when 14-mer primers were used, and the next correct dNTP was included in the complex. All crystals were obtained using Ca^{2+} as the prosthetic metal ion. A dideoxy-terminated primer containing ddC at position 14 was used because of elongation observed during crystallization with a normal 14-mer primer (O^6-BzG:G structure described below). Two data sets obtained from two different crystals that were grown under identical experimental conditions (different drops) provided two different conformations for pddC-14 (O^6-BzG:ddC-1 and O^6-BzG:ddC-2) (Table 3). The first structure (O^6-BzG:ddC-1) revealed a "wobble" pairing between ddC and O^6-BzG, essentially identical to what was observed previously with O^6-MeG (Fig. 6*A*) (25). Three calcium ions are coordinated in the O^6-BzG:ddC-1 structure: two in the active site for catalysis and dNTP coordination and a third coordinated by the thumb domain of Dpo4 and the phosphate group linking the 12th and 13th primer residues. The second structure moves the 14th base into a noninstructional conformation that places it in the growing minor groove (Fig. 7*A*). Superimposition of the O^6-BzG:14ddC1 and O^6-BzG:14ddC2 structures (r.m.s. deviation = 0.344) reveals almost no changes between the complexes outside of that observed

TABLE 2
Pre-steady-state kinetic parameters for 1-base incorporation by Dpo4

Oligomer pair	Template base	dNTP	k_{pol}	$K_{D,dNTP}$	$k_{pol}/K_{D,dNTP}$
			s^{-1}	μM	$s^{-1}\ mM^{-1}$
13-mer 18-mer-1	-G-	dCTP	0.78 ± 0.08[a]	114 ± 54[a]	6.8[a]
13-mer 18-mer-1	-O^6-BzG-	dCTP	0.14 ± 0.01	1300 ± 270	0.11
13-mer 18-mer-1	-O^6-BzG	dTTP	ND[b]	ND	ND
14-mer 18-mer-1	-C -O^6-BzGT-	dATP	0.50 ± 0.03	530 ± 80	0.94
14-mer 18-mer-1	-T -O^6-BzGT-	dATP	0.25 ± 0.01	880 ± 480	0.28

[a] Data from Ref. 25.
[b] ND, not determined due to lack of sufficient product formation in the first binding event.

TABLE 3
Crystal data and refinement parameters

Parameter	O^6-BzG:ddC-1	O^6-BzG:ddC-2	O^6-BzG:T	O^6-BzG:G
X-ray source	APS	APS	NSLS	APS
Beamline	ID5	ID22	X25	ID22
Detector	MAR CCD	MAR CCD	Quantum CCD	MAR CCD
Wavelength (Å)	0.92	0.99	0.98	0.99
Temperature (K)	110	110	110	110
No. of crystals	1	1	1	1
Space group	$P2_12_12$	$P2_12_12$	$P2_12_12$	$P2_12_12$
Unit cell (*a*, *b*, *c*) (Å)	94.0,102.7,52.9	93.1,103.2,52.6	94.5,103.7,52.6	95.2,103.8,52.7
Resolution range (Å)	29.0-2.17	46.5-2.38	29.1-2.39	47.0-1.86
Highest resolution shell[a]	(2.24-2.17)	(2.52-2.38)	(2.49-2.39)	1.93-1.86
No. of measurements	198455	145389	306992	330479
No. of unique reflections	27743 (2695)	20833 (3081)	20842 (3021)	44116 (2209)
Redundancy	7.2 (7.2)	7.0 (6.5)	14.7 (7.5)	7.5 (3.8)
Completeness (%)	99.7 (94.7)	98.7 (93.2)	99.0 (95.5)	98.5 (87.9)
***R*-merge**[b] **(%)**	6.4	9.7	7.6	6.7
Signal/noise ($I/\sigma I$)	19.4 (4.5)	25.5 (2.2)	42.9 (2.2)	38.3 (1.7)
Solvent content (%)	53.1	50.5	51.0	54.4
Model composition				
No. of amino acid residues	342	342	343	341
No. of water molecules	185	104	125	171
No. of Ca^{2+} ions	3	4	4	4
No. of template nucleotides	16	17	16	18
No. of primer nucleotides	14	14	14	15
No. of dGTP	1	1	1	1
R_f[c] **(%)**	23.0	22.6	23.6	23.8
***R*-free**[d] **(%)**	26.7	26.3	27.1	26.5
Estimated coordinate error (Å)				
From Luzatti plot	0.30	0.33	0.36	0.27
From Luzatti plot (*c*-*v*)[e]	0.36	0.38	0.44	0.31
From σA plot	0.27	0.30	0.34	0.23
From σA plot (*c*-*v*)[e]	0.34	0.33	0.43	0.22
Temperature factors				
From Wilson plot ($Å^2$)	42.4	52.2	54.9	32.9
Mean isotropic ($Å^2$)	39.5	48.5	48.4	37.6
r.m.s. deviation in temperature factors				
Bonded main chain atoms ($Å^2$)	1.38	1.37	1.42	1.36
Bonded side chain atoms ($Å^2$)	2.12	2.18	2.16	2.01
r.m.s. S.D. from ideal values				
Bond lengths (Å)	0.008	0.007	0.007	0.006
Bond angles (degrees)	1.6	1.4	1.5	1.3
Dihedral angles (degrees)	22.2	22.2	23.8	22.1
Improper angles (degrees)	1.79	2.86	3.39	2.93

[a] Values in parentheses correspond to the highest resolution shells.
[b] R-merge $= \Sigma_{hkl}\Sigma_j = {}_{1,N}|\langle I_{hkl}\rangle - I_{hkl,j}|/\Sigma_{hkl}\Sigma_j = {}_{1,N}|I_{hkl,j}|$, where the outer sum (*hkl*) is taken over the unique reflections.
[c] $R_f = \Sigma_{hkl}||F_{o,hkl}| - k|F_{c,hkl}||/\Sigma_{hkl}|F_{o,hkl}|$, where $|F_{o,hkl}|$ and $|F_{c,hkl}|$ are the observed and calculated structure factors, respectively.
[d] R_{free} *idem*, for the set of reflections (5% of the total) omitted from the refinement process.
[e] Cross-validation.

with the 14th residue in the primer strand. The only other notable difference between these two structures is the addition of a fourth calcium ion to the active site of Dpo4. The fourth calcium ion is coordinated between the α-phosphate group of the incoming dGTP and the phosphate linking p13C with p14ddC-2 (Fig. 7*A*).

Postinsertion Ternary Complex for "Incorrect" Bypass of O^6-BzG—Crystallization with a 14-mer primer containing thymidine at the 3′ terminus (pT14) was performed in the presence of dGTP and calcium. The resulting crystals diffracted to 2.4 Å resolution. Following molecular replacement without a 13-residue primer DNA in the model, difference maps revealed substantial positive density regions that corresponded to the phosphate group for the 14th nucleotide and some density corresponding to the pyrimidine ring of thymidine. However, much of the density for pT14 near the glycosidic bond and in the ribose is absent, indicating a high level of disorder for the thymidine. A disordered pT14 is quite similar to what was observed previously with Dpo4 in a ternary complex with O^6-MeG-modified DNA, but in the O^6-BzG:T structure the density is convincing enough to limit pT14 to one conformation, namely a pseudo-Watson-Crick geometry (Fig. 6*B*). A fourth calcium ion is coordinated between the α-phosphate group of the incoming dGTP and the phosphate linking p13C with p14T, similar to what was observed with O^6-BzG:14ddC2 and O^6-BzG:G.

Postinsertion Ternary Complex Containing +1 Frameshift—Initial attempts to obtain crystals containing the O^6-BzG:C pair

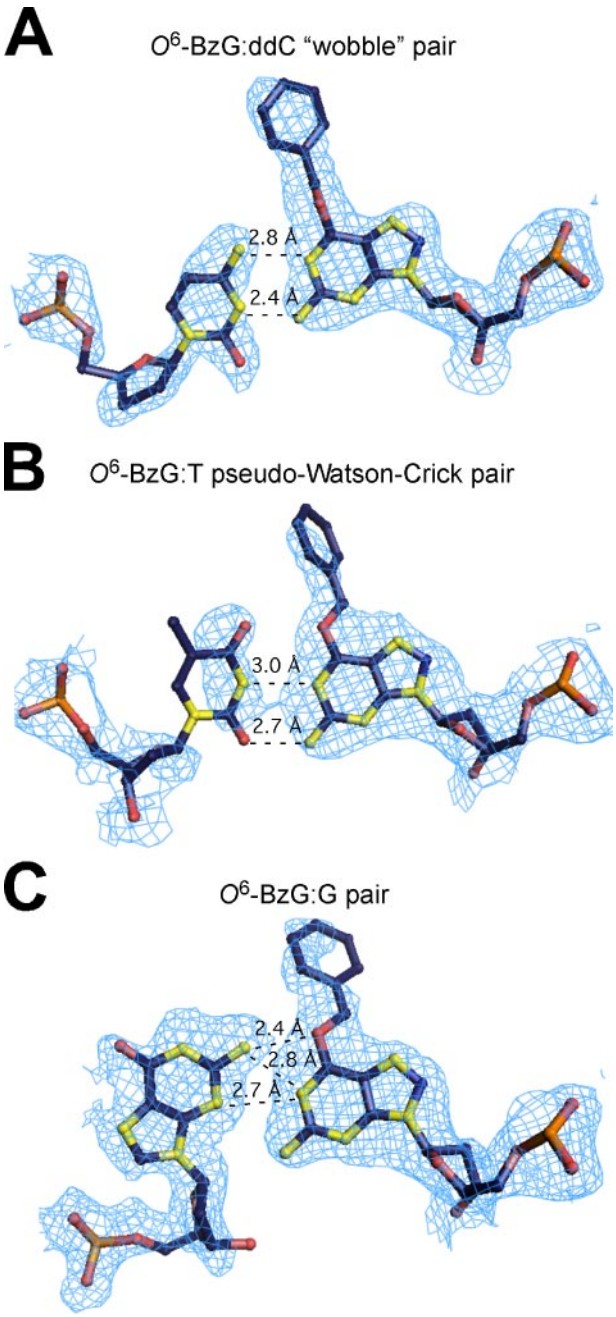

FIGURE 6. **Comparative base pairing orientations opposite *O*⁶-BzG at the catalytic center of the ternary complexes.** *A*, the 14th nucleotide ddC forms a "wobble" base pair with template *O*⁶-BzG in the *O*⁶-BzG:ddC-1 structure. *B*, the 14th nucleotide T from the *O*⁶-BzG:T structure is positioned in a pseudo-Watson-Crick pair. *C*, Dpo4-catalyzed incorporation of dGTP into the primer strand during crystallization places pG15 opposite *O*⁶-BzG in the *O*⁶-BzG:G structure. Carbon atoms are shown as *dark blue*, nitrogen atoms as *yellow*, and oxygen atoms as *red*. The electron density map (*marine mesh*) $3F_o - 2F_c$ is contoured at the 1σ level.

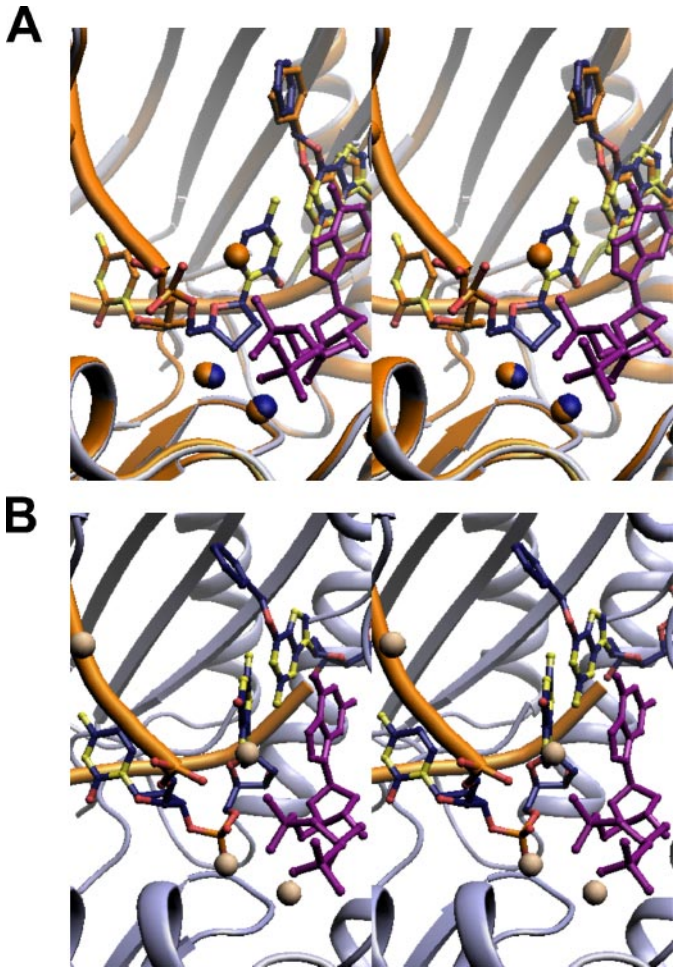

FIGURE 7. **Comparison of primer ddC orientations in the *O*⁶-BzG:ddC-1 and *O*⁶-BzG:ddC-2 structures and a view of the *O*⁶-BzG:G active site.** *A*, stereo view of the superimposed (r.m.s. deviation = 0.344) *O*⁶-BzG:ddC-1 (Dpo4 (*light blue*) and nucleotides and ions (*dark blue*)) and *O*⁶-BzG:ddC-2 (Dpo4, ions, and nucleotides (*orange*)) structures. Dpo4 is shown in *schematic diagram form* for both structures. The incoming dGTP (*magenta*) from the *O*⁶-BzG:ddC-1 structure is shown in *ball and stick form*. The 14th nucleotide (*dark blue*, ddC) from the *O*⁶-BzG:ddC-1 structure forms a wobble pair with *O*⁶-BzG, but the 14th nucleotide (*orange*, ddC) from the *O*⁶-BzG:ddC-2 ternary complex is moved into a noninstructional conformation. *B*, stereo view of the *O*⁶-BzG:G active site. Dpo4 (*light blue*) is shown in *schematic diagram form*. The last two primer residues, p14C and p15G, and the *O*⁶-BzG lesion are shown in *ball and stick form* (*dark blue*). The 14th base in the primer, p14C, is placed in a conformation similar to that observed in the *O*⁶-BzG:ddC-2 structure. The calcium ions (*light brown*) and incoming dGTP (*magenta*) are also shown.

gave crystals that diffracted to 1.86 Å with excellent completeness and R_{merge} values. Following molecular replacement, it was apparent that an additional base had been added to the 14-dC primer terminus. During the crystallization process (in the presence of calcium) Dpo4 had incorporated a single G into the primer, generating a 15-mer that terminated with dG. The p14C residue was placed in a noninstructional orientation similar to the *O*⁶-BzG:ddC-2 structure, and the newly inserted pG15 remained in the *anti* conformation (Fig. 7*B*). Three hydrogen bonds are formed between pG15 and *O*⁶-BzG: one between the N3 atom of pG15 and the N2 exocyclic amine of *O*⁶-BzG and a second bifurcated pairing between the N2 exocyclic amine of pG15 and the N1 and O6 atoms of *O*⁶-BzG (Fig. 6*C*). The incoming dGTP remains coordinated by two calcium ions in the Dpo4 active site. A fourth calcium ion is coordinated between the α-phosphate group of the incoming dGTP and the phosphate linking p14C with p15G and also with the O6 atom of pG15.

DISCUSSION

Covalent modification of DNA, excluding that involved in regulatory or epigenetic purposes, can result in varying degrees of cellular dysfunction dependent upon the amount and the type of damage incurred (1). Studying the mechanism(s) of

translesion synthesis utilized by DNA polymerases can provide information regarding how mutations are formed and what factors determine the level of mutagenesis observed in the cell. The effect of lesion size upon Dpo4 catalysis was probed by studying bypass of O^6-BzG. The results obtained herein expand and extend previous work with O^6-MeG, a known mutagenic lesion.

The kinetic analyses reported here are consistent with the hypothesis that increasing the size of the O^6-alkylG adducts decreases the efficiency of Dpo4 catalysis opposite the lesion, but the steady-state fidelity of bypass was increased slightly compared with the smaller O^6-MeG (25). Under steady-state conditions, Dpo4-catalyzed insertion of dCTP opposite O^6-BzG was inhibited 5-fold relative to bypass of O^6-MeG. In the pre-steady state, O^6-BzG inhibition was 4-fold less efficient than Dpo4-catalyzed bypass of O^6-MeG. However, it is important to remember that "correct" bypass of both O^6-MeG and O^6-BzG is inhibited 14- and 62-fold relative to Dpo4-catalyzed insertion of dCTP opposite unmodified G (comparing pre-steady-state data). Thus, Dpo4 is not very efficient at bypass of either O^6-MeG or O^6-BzG. Generally speaking, the steady-state results for misincorporation events (T, A, or G incorporation) indicate that Dpo4 is an order of magnitude less efficient at incorrect bypass of O^6-BzG compared with O^6-MeG, and the LC-MS analyses lend support to the trends observed in the kinetic parameters ($C > T \sim A \gg G$).

The structural analysis of Dpo4-catalyzed bypass of O^6-BzG is similar to the results reported for O^6-MeG. The mode of "correct" bypass also occurs through a O^6-BzG:ddC wobble pair, reinforcing previous conclusions about pairing of an O^6-alkylG adduct with polymerase, although a second "noninstructional" conformation was observed that moves ddC down into the growing minor groove (Fig. 7*A*). The noninstructional conformation observed in the O^6-BzG:ddC-2 structure may reflect an effect of the added bulk of the benzyl group that destabilizes the wobble pairing between O^6-BzG and C. Superimposition of the O^6-BzG:ddC-1 and O^6-MeG:C structures (r.m.s. deviation = 0.351) shows that the increased size of the benzyl adduct is accommodated in the cleft between the thumb and little finger domains with essentially no alterations in amino acid side chain conformations or protein-DNA contacts. The methylene group in the O^6-BzG:14ddC1 structure extends out from the O6 atom perpendicular to the purine ring system of the O^6-BzG residue, as opposed to the proximal orientation observed with O^6-MeG:C.

The O^6-BzG:T pair is found in a pseudo-Watson-Crick orientation that provides two hydrogen bonding partners between the bases, but it also places the two exocyclic oxygen atoms in close proximity to one another (3.1 Å apart). The benzyl group is placed in a proximal position relative to the purine ring system, and the added repulsion between the O6 atom of O^6-BzG and the O4 atom of T probably plays a role in the disorder that is observed near pT14, as well as the resultant favoring of dCTP insertion during Dpo4-catalyzed bypass of O^6-BzG. Alignment of the O^6-BzG:T structure with the O^6-BzG:14ddC1 structure shows that pT14 is shifted further into the major groove relative to p14ddC-1 (Fig. 8). The BzG residues are changed slightly between the 14ddC-1 and T structures, with the exocyclic O4 atom of T pushing the benzyl group into a more proximal orientation relative to the purine ring system (Fig. 8).

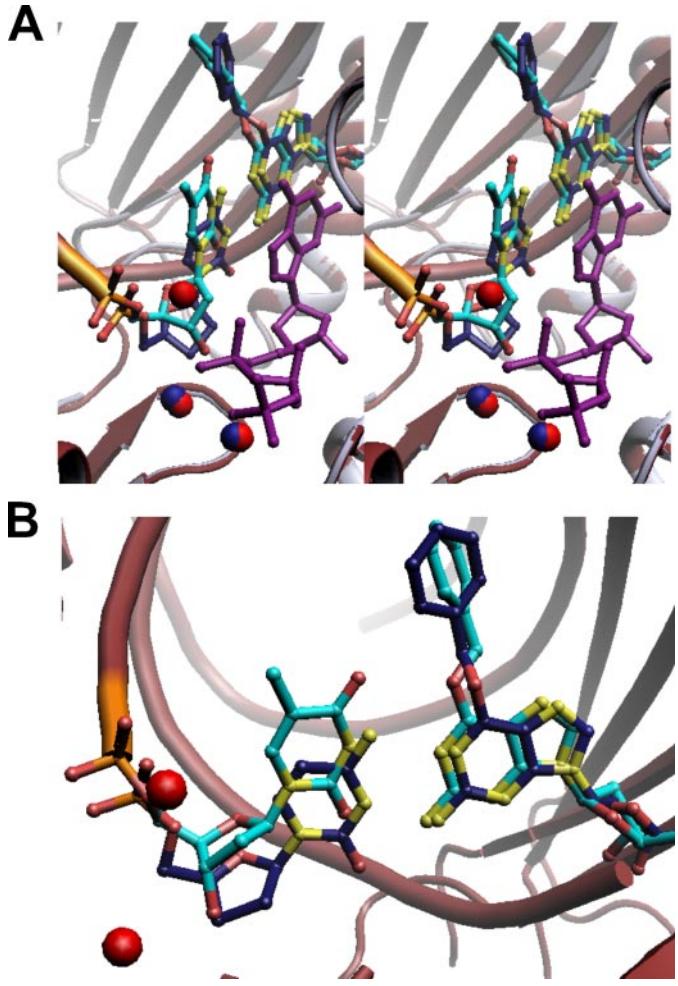

FIGURE 8. **View of the O^6-BzG:T active site superimposed on the wobble O^6-BzG:ddC-1 pair.** *A*, stereo view of the active site from the O^6-BzG:T ternary complex is shown superimposed on the O^6-BzG:ddC-1 structure (r.m.s. deviation = 0.390) with Dpo4 in *schematic diagram form* (O^6-BzG:T (*ruby*), O^6-BzG:ddC-1 (*light blue*)). The O^6-BzG:T pair is shown with *cyan* carbon atoms, and the O^6-BzG:ddC-1 wobble pair is shown with *dark blue* carbon atoms. The O^6-BzG:T calcium ions are *red*, and the O^6-BzG:ddC-1 calcium ions are *dark blue*. The incoming dGTP from the O^6-BzG:T structure is shown in *ball and stick form* (*magenta*). *B*, the p14T residue (*cyan* carbon atoms) is shifted up in the active site relative to p14ddC-1 (*dark blue* carbon atoms), and the benzyl group in the O^6-BzG:T structure is shifted slightly toward the proximal orientation.

Additional structures obtained with O^6-BzG-modified DNA provides insights into how Dpo4 can "slip" on the template and accommodate three bases in the polymerase active site to generate a +1 frameshift. The frameshift was not manifested in the full-length extension products (analyzed by LC-MS/MS) (Fig. 3 and supplemental Figs. S4–S8), presumably because the 3′-hydroxyl group of the newly inserted pG15 is too far removed from the catalytic center for phosphoryl transfer to proceed. In the O^6-BzG:G structure, the p14C normally paired opposite O^6-BzG during "correct" bypass is flipped down into the DNA binding cleft (Fig. 7*A*), with a single G (p15G) inserted opposite O^6-BzG (Fig. 7*B*). The purine ring of p15G remains in the *anti* conformation but is shifted up, with the N3 atom of p15G forming a hydrogen bond with the N2 exocyclic amine of O^6-BzG,

and the N2 exocyclic amine of p15G is in a bifurcated pairing orientation with the N1 and O6 atoms of O^6-BzG (Fig. 6*C*).

Studies with model replicative polymerases, such as pol T7$^-$ and HIV-1 RT, have shown that the O^6-BzG moiety is a greater block to polymerase efficiency than the smaller O^6-MeG lesion, with O^6-MeG being slightly more miscoding than O^6-BzG for both enzymes (16). In the pre-steady-state analysis for HIV-1 RT, catalysis opposite O^6-alkylG was inhibited primarily at the stage of nucleotide binding for both accurate and mutagenic bypass (16). Dpo4, on the other hand, has a slower k_{pol} for bypass of both O^6-MeG and O^6-BzG (Table 2). The decrease in Dpo4 catalytic efficiency observed between O^6-MeG and O^6-BzG is determined by a much higher $K_{D,dNTP}$ for O^6-BzG. The lower binding affinity is not surprising, because the bulk of the benzyl moiety extending out of the DNA binding cleft is more likely to impede binding of any dNTP opposite O^6-BzG than the addition of a methyl group.

The previous work on pol T7$^-$ and HIV-1 RT-catalyzed bypass of O^6-MeG and O^6-BzG led to the proposal that some fraction of both pol T7$^-$ and HIV-1 RT could proceed through a reversible inactive or nonproductive form. The results obtained herein illustrate a fundamental difference between Dpo4 and the aforementioned model polymerases that is likely to be related to polymerase structure and the processivity conferred by said structure. As opposed to the nonproductive complexes observed with polymerases such as pol T7$^-$ and HIV-1 RT, Dpo4 catalysis opposite O^6-BzG is simply slower and requires more dNTP to move the reaction forward. There is some indication that distinct changes in the finger domain of HIV-1 RT may play a role in determining an active *versus* an inactive state (34), but the lack of any O^6-alkylG-modified DNA and thiol-based covalent modification of the complexes in question render such a suggestion speculative at best. Structural evidence of the nonproductive complex has not been obtained for pol T7$^-$; however, evidence linking different conformational changes of the pol T7$^-$ finger domain to either correct or incorrect bypass may be indicative of what is occurring during pol T7$^-$-catalyzed bypass of O^6-BzG (35). In this respect, Dpo4 may have the advantage of no major conformational rearrangements during O^6-alkylG bypass, so that Dpo4 is not likely to stall by entering a state that is more stable, energetically speaking, than the transition state but not catalytically competent. The disadvantage for Dpo4 is the nonprocessive nature of the enzyme, because reducing k_{pol} effectively drives the kinetic partitioning between k_{pol} and k_{off} toward dissociation and, in the case of Dpo4, results in a decrease in the burst amplitude.

The question remains open as to which type of polymerase is encountering the O^6-alkylG-modified DNA in the cell, but the answer could be related to which polymerase is most strongly inhibited by O^6-alkylG lesions. Comparing steady-state catalytic efficiencies, human pol δ and η appear to be inhibited in roughly the same manner by both O^6-MeG (~10-fold) and O^6-BzG (~100-fold) relative to correct bypass on unmodified DNA (18). Pre-steady-state kinetic analyses indicate that HIV-1 RT incorporation of either dCTP or dTTP opposite O^6-MeG is inhibited 7–8-fold, respectively, relative to dCTP incorporation opposite unmodified G (16), which is comparable with the 14-fold inhibition observed for Dpo4 (25). The O^6-BzG lesion inhibits HIV-RT incorporation of either dCTP or dTTP ~70–100-fold, respectively, relative to the control reaction (16). Both of these values indicate that HIV-RT can bypass O^6-alkylG-modified DNA without suffering a greater degree of inhibition than Dpo4, a model for translesion synthesis.

Another comparison can be made between Dpo4 and pol T7$^-$-catalyzed bypass of O^6-alkylG-modified DNA. Compared with the steady-state values observed with Dpo4, mutagenic bypass of O^6-MeG and O^6-BzG by pol T7$^-$ is less perturbed than any catalytic event that Dpo4 attempts opposite the lesions, with the exception of Dpo4-catalyzed insertion of dCTP opposite O^6-MeG (25). Direct comparison of the k_{cat}/K_m values for insertion opposite O^6-alkylG indicates that pol T7$^-$ is actually ~4-fold more efficient in inserting dTTP opposite O^6-MeG than Dpo4-catalyzed incorporation of dCTP opposite O^6-MeG and ~3-fold more efficient in inserting dTTP opposite O^6-BzG than Dpo4-catalyzed incorporation of dCTP opposite the benzyl lesion. Granted that these are enzymes from disparate systems, nevertheless these data may imply that many of the smaller lesions may never be encountered by the Y-family polymerases because the replication machinery can copy past them without too much difficulty. Only when very bulky lesions are encountered, which replicative polymerases simply cannot bypass, do the Y-family polymerases have an opportunity to perform translesion synthesis; hence, the existence of alternate repair pathways for small lesions such as O^6-MeG and 8-oxo-7,8-dihydroguanine.

The major difference observed between Dpo4 and the replicative polymerases (pol δ, pol T7$^-$, and HIV-1 RT) is that Dpo4 bypasses O^6-MeG and O^6-BzG relatively accurately. Presumably, the open and flexible active site of Dpo4 allows formation of the wobble pair to occur in a facile manner, and the same features allow the repulsion of the exocyclic oxygen atoms in the O^6-BzG:T pair to prevent incorporation of dTTP. The rigid constraints found in the active site of replicative polymerases may be inclined to force O^6-alkylG:T pairs into a more enclosed, geometrically intolerant environment, which results in a greater fraction of dTTP incorporated relative to what occurs during Dpo4-catalyzed bypass. Recent crystal structures track the prokaryotic model polymerase BF from *Bacillus stearothermophilus* and are consistent with such a view (36). The accurate or "correct" bypass of O^6-MeG by BF appears to favor Watson-Crick geometry between O^6-MeG and a protonated C. Notably, the wobble pairing scheme is only observed *after* the O^6-MeG:C pair has been processed to a more solvent-accessible position (−10-position) relative to the BF active site. Mutagenic replication by BF occurs primarily through pseudo-Watson-Crick geometry between O^6-MeG and T, which is similar but not identical to what is observed with Dpo4. An unusual electrostatic interaction between the O4 atom of T and the methyl protons of O^6-MeG was observed at every stage of BF-catalyzed replication (active site, −1 and −2 postinsertion sites) and was proposed to increase the stability of the O^6-MeG:T pair. The reported catalytic efficiencies of dCTP and dTTP incorporation opposite O^6-MeG by BF were decreased ~100,000- and ~10,000-fold, respectively, relative to dCTP incorporation opposite unmodified G, much greater than the

changes in efficiency observed with Dpo4 or HIV-RT (comparing pre-steady-state values). The kinetic analysis indicates that BF insertion of dTTP opposite O^6-MeG is ~11-fold more efficient than dCTP incorporation opposite O^6-MeG. The large decrease in BF catalytic efficiency is difficult to reconcile with work from our own group but appears to be dependent upon a substantial decrease in the reaction rate (*i.e.* k_{pol} is ~1600- and ~400-fold slower for dCTP and dTTP incorporation opposite O^6-MeG relative to a control reaction, whereas nucleotide binding affinity is decreased ~60 to ~100-fold for accurate and mutagenic bypass, respectively) (36).

The general conclusions derived here are consistent with the idea that increasing adduct size decreases polymerase efficiency, as has been observed with many polymerases (16, 17, 28, 37, 38), although some instances of greater tolerance have been reported, such as pol η bypass of O^6-PobG and pol κ bypass of N^2-alkylG adducts (18, 39). The fidelity of Dpo4 catalysis remains largely unaltered between O^6-MeG- and O^6-BzG-modified DNA, and the more accurate mechanism of O^6-alkylG bypass distinguishes Dpo4 from most other polymerases studied to date. Comparing studies with Dpo4 to those with BF indicates that, in a simplistic sense, the accuracy of O^6-alkylG bypass is related to how well the active site of a given polymerase tolerates the wobble pair between O^6-alkylG and C.

Acknowledgments—We thank H. Robinson for data collection support at the National Synchrotron Light Source; Z. Jin, P. S. Pallan, and Z. Wawrzak for data collection support at the Advanced Photon Source; I. D. Kozekov for synthesis of the O^6-BzG-modified oligonucleotides; and K. Trisler for assistance in preparation of the manuscript.

REFERENCES

1. Friedberg, E. C., Walker, G. C., Siede, W., Wood, R. D., Shultz, R. A., and Ellenberger, T. (2006) *DNA Repair and Mutagenesis*, 2nd Ed., American Society for Microbiology Press, Washington, D. C.
2. Margison, G. P., Santibanez Koref, M. F., and Povey, A. C. (2002) *Mutagenesis* **17,** 483–487
3. Wyatt, M. D., and Pittman, D. L. (2006) *Chem. Res. Toxicol.* **19,** 1580–1594
4. Lawley, P. D. (1984) in Searle, C. E. (ed) *Chemical Carcinogens*, 2nd Ed., American Chemical Society, Washington, D. C.
5. Loveless, A. (1969) *Nature* **223,** 206–207
6. Quinn, J. A., Desjardins, A., Weingart, J., Brem, H., Dolan, M. E., Delaney, S. M., Vredenburgh, J., Rich, J., Friedman, A. H., Reardon, D. A., Sampson, J. H., Pegg, A. E., Moschel, R. C., Birch, R., McLendon, R. E., Provenzale, J. M., Gururangan, S., Dancey, J. E., Maxwell, J., Tourt-Uhlig, S., Herndon, J. E., II, Bigner, D. D., and Friedman, H. S. (2005) *J. Clin. Oncol.* **23,** 7178–7187
7. Lindahl, T. (1993) *Nature* **362,** 709–715
8. Pegg, A. E., Dolan, M. E., Scicchitano, D., and Morimoto, K. (1985) *Environ. Health Perspect.* **62,** 109–114
9. Pegg, A. E., Roberfroid, M., von Bahr, C., Foote, R. S., Mitra, S., Bresil, H., Likhachev, A., and Montesano, R. (1982) *Proc. Natl. Acad. Sci. U. S. A.* **79,** 5162–5165
10. Yoshioka, K., Yoshioka, Y., and Hsieh, P. (2006) *Mol. Cell* **22,** 501–510
11. Langston, L. D., and O'Donnell, M. (2006) *Mol. Cell* **23,** 155–160
12. Haracska, L., Prakash, S., and Prakash, L. (2000) *Mol. Cell Biol.* **20,** 8001–8007
13. Singh, J., Su, L., and Snow, E. T. (1996) *J. Biol. Chem.* **271,** 28391–28398
14. Tan, H. B., Swann, P. F., and Chance, E. M. (1994) *Biochemistry* **33,** 5335–5346
15. Voigt, J. M., and Topal, M. D. (1995) *Carcinogenesis* **16,** 1775–1782
16. Woodside, A. M., and Guengerich, F. P. (2002) *Biochemistry* **41,** 1027–1038
17. Woodside, A. M., and Guengerich, F. P. (2002) *Biochemistry* **41,** 1039–1050
18. Choi, J.-Y., Chowdhury, G., Zang, H., Angel, K. C., Vu, C. C., Peterson, L. A., and Guengerich, F. P. (2006) *J. Biol. Chem.* **281,** 38244–38256
19. Fiala, K. A., and Suo, Z. (2004) *Biochemistry* **43,** 2116–2125
20. Fiala, K. A., and Suo, Z. (2004) *Biochemistry* **43,** 2106–2115
21. Ling, H., Boudsocq, F., Plosky, B. S., Woodgate, R., and Yang, W. (2003) *Nature* **424,** 1083–1087
22. Ling, H., Boudsocq, F., Woodgate, R., and Yang, W. (2001) *Cell* **107,** 91–102
23. Ling, H., Boudsocq, F., Woodgate, R., and Yang, W. (2004) *Mol. Cell* **13,** 751–762
24. Ling, H., Sayer, J. M., Plosky, B. S., Yagi, H., Boudsocq, F., Woodgate, R., Jerina, D. M., and Yang, W. (2004) *Proc. Natl. Acad. Sci. U. S. A.* **101,** 2265–2269
25. Eoff, R. L., Irimia, A., Egli, M., and Guengerich, F. P. (2007) *J. Biol. Chem.* **282,** 1456–1467
26. Autrup, H., and Stoner, G. D. (1982) *Cancer Res.* **42,** 1307–1311
27. Peterson, L. A. (1997) *Chem. Res. Toxicol.* **10,** 19–26
28. Choi, J.-Y., and Guengerich, F. P. (2006) *J. Biol. Chem.* **281,** 12315–12324
29. Zang, H., Goodenough, A. K., Choi, J. Y., Irimia, A., Loukachevitch, L. V., Kozekov, I. D., Angel, K. C., Rizzo, C. J., Egli, M., and Guengerich, F. P. (2005) *J. Biol. Chem.* **280,** 29750–29764
30. Christian, N. P., Reilly, J. P., Mokler, V. R., Wincott, F. E., and Ellington, A. D. (2001) *J. Am. Soc. Mass Spectrom.* **12,** 744–753
31. Kabsch, W. (1988) *J. Appl. Crystallogr.* **21,** 916–924
32. Otwinowski, Z., and Minor, W. (1997) *Methods Enzymol.* **276,** 307–326
33. Brunger, A. T., Adams, P. D., Clore, G. M., DeLano, W. L., Gros, P., Grosse-Kunstleve, R. W., Jiang, J. S., Kuszewski, J., Nilges, M., Pannu, N. S., Read, R. J., Rice, L. M., Simonson, T., and Warren, G. L. (1998) *Acta. Crystallogr. Sect. D Biol. Crystallogr.* **54,** 905–921
34. Huang, H., Harrison, S. C., and Verdine, G. L. (2000) *Chem. Biol.* **7,** 355–364
35. Tsai, Y. C., and Johnson, K. A. (2006) *Biochemistry* **45,** 9675–9687
36. Warren, J. J., Forsberg, L. J., and Beese, L. S. (2006) *Proc. Natl. Acad. Sci. U. S. A.* **103,** 19701–19706
37. Choi, J.-Y., and Guengerich, F. P. (2004) *J. Biol. Chem.* **279,** 19217–19229
38. Choi, J.-Y., and Guengerich, F. P. (2005) *J. Mol. Biol.* **352,** 72–90
39. Choi, J.-Y., Angel, K. C., and Guengerich, F. P. (2006) *J. Biol. Chem.* **281,** 21062–21072